ACS APPLIED MATERIALS & INTERFACES

Research Article

www.acsami.org

Coin-like α-Fe_2O_3@$CoFe_2O_4$ Core–Shell Composites with Excellent Electromagnetic Absorption Performance

Hualiang Lv,[†] Xiaohui Liang,[‡] Yan Cheng,[‡] Haiqian Zhang,[†] Dongming Tang,[†] Baoshan Zhang,*[,†] Guangbin Ji,*[,‡] and Youwei Du[§]

[†]School of Electronic Science and Engineering, Nanjing University, Nanjing 210093, P. R. China

[‡]College of Material Science and Technology, Nanjing University of Aeronautics and Astronautics, Nanjing 210016, P. R. China

[§]Laboratory of Solid State Microstructures, Nanjing University, Nanjing 210093, P. R. China

ABSTRACT: In this paper, we designed a novel core–shell composite for microwave absorption application in which the α-Fe_2O_3 and the porous $CoFe_2O_4$ nanospheres served as the core and shell, respectively. Interestingly, during the solvothermal process, the solvent ratio (V) of PEG-200 to distilled water played a key role in the morphology of α-Fe_2O_3 for which irregular flake, coin-like, and thinner coin-like forms of α-Fe_2O_3 can be produced with the ratios of 1:7, 1:3, and 1:1, respectively. The porous 70 nm diameter $CoFe_2O_4$ nanospheres were generated as the shell of α-Fe_2O_3. It should be noted that the $CoFe_2O_4$ coating layer did not damage the original shape of α-Fe_2O_3. As compared with the uncoated α-Fe_2O_3, the Fe_2O_3@$CoFe_2O_4$ composites exhibited improved microwave absorption performance over the tested frequency range (2–18 GHz). In particular, the optimal reflection loss value of the flake-like composite can reach −60 dB at 16.5 GHz with a thin coating thickness of 2 mm. Furthermore, the frequency bandwidth corresponding to the RL_{min} value below −10 dB was up to 5 GHz (13–18 GHz). The enhanced microwave absorption properties of these composites may originate from the strong electron polarization effect (i.e., the electron polarization between Fe and Co) and the electromagnetic wave scattering on this special porous core–shell structure. In addition, the synergy effect between α-Fe_2O_3 and $CoFe_2O_4$ also favored balancing the electromagnetic parameters. Our results provided a promising approach for preparing an absorbent with good absorption intensity and a broad frequency that was lightweight.

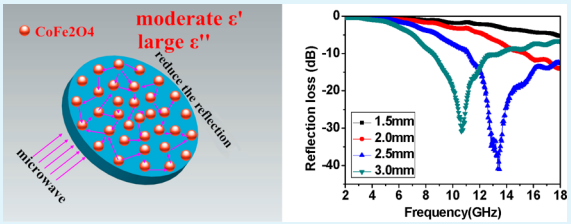

KEYWORDS: *α-Fe_2O_3, α-Fe_2O_3@$CoFe_2O_4$, core–shell structure, microwave absorption properties, lightweight absorber*

1. INTRODUCTION

Microwave absorption materials have attracted a great deal of attention because of the growth in the utilization of wireless equipment, mobile phones, and radar systems.[1−3] It is well-known that the microwave absorbent is a type of functional material that can effectively absorb an electromagnetic wave and attenuate it in the form of thermal energy by magnetic or dielectric loss.[4] Thus, microwave absorption materials are mainly divided into two types depending on how they attenuate the electromagnetic wave.[5,6] Sometimes, a single magnetic loss or dielectric loss material cannot simultaneously meet the requirements of having a thin coating thickness and a broad absorption bandwidth and being lightweight.[7] Therefore, to achieve novel absorption properties, much effort has been devoted to combining two or more kinds of functional materials to adjust the electromagnetic parameters for achieving a desired reflection loss (RL) value. For example, magnetic loss-based composites, including Ag@Ni,[8] Co@MnO_2,[9] Fe/SiO_2,[10,11] Fe_3O_4@ZnO,[12] Fe_3O_4@TiO_2,[13−15] and Fe_3O_4@poly(3,4- ethylenedioxythiophene),[16] carbon-based composites like FeCo/C[17,18] reduced graphene oxide (RGO)–$MnFe_2O_4$ nanocomposites,[19] graphene/$NiFe_2O_4$,[20] and RGO/$CoFe_2O_4$[21] have been reported in recent years. It is worth noting that the interesting three-dimensional (3D) SiO_2@Fe_3O_4 core–shell nanorod array–graphene architecture had been synthesized as a representative magnetically based absorbent, and the optimal reflection loss value can reach −31.9 dB at a thickness of 2.5 mm.[22] As a result, we may conclude that the enhanced microwave absorption performance of these composites may originate from the improved impedance matching properties caused by the balancing of the complex permittivity and permeability perfectly.[23,24] More importantly, the interface between different materials may form a new type of bond that is also attributed to the electron polarization and results in an increase in the level of electromagnetic attenuation.

Currently, Fe_2O_3-based microwave absorbents have been attractive because of their high chemical stability, environmentally friendly nature, and low cost.[25,26] In fact, pure Fe_2O_3 has a lower real part permittivity value (3–5) that is apt to yield high impedance matching. However, the poor attenuation ability has been the major shortcoming of the EMA materials because of the lower ε'' value. Therefore, a solution is to mix

Received: December 2, 2014
Accepted: February 9, 2015
Published: February 9, 2015

DOI: 10.1021/am508438s
ACS Appl. Mater. Interfaces 2015, 7, 4744–4750

Fe_2O_3 with another material that exhibits strong attenuation ability but poor impedance matching. For instance, Chen et al. successfully loaded the Fe_2O_3 nanoparticles into the multiwalled carbon nanotubes and found that the composite exhibited an excellent microwave absorption properties with a minimal reflection loss value of −32.7 dB under a coating thickness of 2.7 mm.[27] Numerous Fe_2O_3 nanosheets with a thin thickness of 5 nm arrayed on the graphene also exhibited improved microwave absorption performance with an optimal RL value of −64.1 dB at a thickness of 4.92 mm.[28] Similarly, the leaf-like Fe_2O_3/polyaniline composite provided an RL value of −50 dB with a thickness of 5.3 mm.[29] Although the strong reflection loss value was exhibited by these Fe_2O_3 composites, the coating thickness is too large. In this paper, we report a new Fe_2O_3-based composite, namely the Fe_2O_3@$CoFe_2O_4$ core−shell composite, which effectively solves this problem. These special core−shell structures have significantly improved the microwave absorption compared with that of the single composition of Fe_2O_3 or $CoFe_2O_4$, especially with a coating thickness of <2 mm.

2. EXPERIMENTAL SECTION

2.1. Materials. Iron nitrate [$Fe(NO)_3$], barium nitrate [$Ba(NO_3)_2$], ferric trichloride ($FeCl_3$), ammonium acetate (NH_4Ac), cobalt acetate [$Co(Ac)_2$], and sodium hydroxide (NaOH) were purchased from Nanjing Chemical Reagent Co. Ethylene glycol (EG) and polyethylene (PEG-200) were purchased from the Sinopharm Chemical Reagent Co. All of the chemical reagents used in this work were analytically pure and used without further purification.

2.2. Synthesis of α-Fe_2O_3. The α-Fe_2O_3 used in this study was prepared by a simple hydrothermal process. Briefly, 8 mmol of $Fe(NO_3)_3$ and 1 mmol of $Ba(NO_3)_2$ were first dissolved in 40 mL of a PEG-200/distilled water mixing solution via mechanical stirring for 15 min until the solution became clear. Then, 2.0 g of NaOH was added to the mixing solution and the mixture stirred for an additional 15 min. After that, the mixed solution was transferred into a Teflon-lined stainless steel autoclave and subsequently sealed and heated at 220 °C for 24 h. Finally, the resulting sample was collected by centrifuge, washed with absolute ethanol and distilled water several times, and dried in a vacuum drying oven at 60 °C for 6 h.

2.3. Synthesis of the α-Fe_2O_3@$CoFe_2O_4$ Core−Shell Structure. The α-Fe_2O_3@$CoFe_2O_4$ composites were prepared by a simple hydrothermal approach. Briefly, 0.2 g of the as-prepared Fe_2O_3 was first dispersed in 60 mL of EG by being stirred for 10 min, followed by addition of $Co(Ac)_2$ (0.25 g), $FeCl_3$ (0.6 g), and NH_4Ac (0.5 g). After being stirred for an additional 10 min, the mixed solution was transferred into a Teflon-lined stainless steel autoclave with a capacity of 100 mL. The autoclave was heated at 200 °C for 24 h and then allowed to cool to room temperature. The final products were washed with ethanol by magnetic decantation four times and dried at 100 °C for 4 h in a vacuum.

2.4. Characterizations. The powder X-ray diffraction (XRD) pattern measurements were taken on a Bruker D8 ADVANCE X-ray diffractometer using Cu Kα radiation (λ = 0.154178 nm) with a scanning voltage of 40 kV, a scanning current of 40 mA, and a scanning range from 20° to 60°. A Hitachi S4800 type scanning electron microscope (operating at an acceleration voltage of 3.0 kV and equipped with an energy dispersive X-ray spectroscope) was used to observe the morphology features and sizes of α-Fe_2O_3 and Fe_2O_3@$CoFe_2O_4$. The morphology of the coin-like composite was further characterized by transmission electron microscopy (TEM) (JEM JEOL 2100). The atomic ratio was tested by inductively coupled plasma (ICP) (Optima 5300 DV). The focused iron beam (FIB) system was utilized to test the shell thickness of the coin-like Fe_2O_3@$CoFe_2O_4$ (FEI versa 3D). The magnetic properties, including coercive force and saturation magnetization, were determined by a vibrating sample magnetometer (VSM, Lakeshore, model 7400 series) at room temperature. The XPS spectrum was measured in a PHI 5000 VersaProbe system with an Al Kα X-ray source operating at 150 W. The S parameter, including S_{11}, S_{12}, S_{21}, and S_{22}, was tested with an Agilent PNA N5224A vector network analyzer using the coaxial-line method by preparing the sample by homogeneous mixing of the paraffin wax and sample (mass ratio of 1:1) and then pressing it into toroidal-shaped samples (Φ_{out} = 7.0 mm, and Φ_{in} = 3.04 mm). Afterward, software that has been installed in Agilent PNA can calculate the ε', ε'', μ', and μ'' values. Finally, the RL values with different thicknesses can be calculated by using the following formulas.[30−32]

$$Z_{in} = Z_0\sqrt{u_r/\varepsilon_r}\,\tanh[j(2\pi fd/c)]\sqrt{u_r\varepsilon_r} \quad (1)$$

$$\mathrm{RL\ (dB)} = 20 \times \log|(Z_{in} - Z_0)/(Z_{in} + Z_0)| \quad (2)$$

where Z_0 represents the impedance of free space, Z_{in} is the input impedance of the absorber, f is the frequency of the electromagnetic wave, d is the coating thickness of the absorber, c is the velocity of the electromagnetic wave in free space, and RL is the minimal reflection loss value. ε_r ($\varepsilon_r = \varepsilon' - j\varepsilon''$) and μ_r ($\mu_r = \mu' - j\mu''$) are the complex permittivity and permeability of the absorber, respectively.

3. RESULTS AND DISCUSSION

Among all the chemical synthesis methods, the solvothermal method has attracted the most attention because of its easy modification of the morphology.[33] During the solvothermal process, many factors, such as the surfactant:molar ratio of the precursor salt can determine and affect the morphology of final products. In this study, the shape and thickness of flake- or coin-like α-Fe_2O_3 can be easily tuned by adjusting the volume ratio (V) between PEG-200 and distilled water. When a volume ratio of 1:7 is maintained in the solvent, the flake-like α-Fe_2O_3 particles (marked in C1) with a thickness of 100 nm are gained while they are not in a regular shape as shown in Figure 1a. Clearly, monodisperse coin-like α-Fe_2O_3 particles (C2) with a uniform shape and size can be obtained (seen Figure 1b) when V is increased to 1:3. From the high-resolution SEM images (Figure 1c,d), one can see that the coin-like particles have a very smooth surface and a narrow thickness range from 4 to 5 μm. The average diameter of these coin-like particles can be confirmed to be 11−13 μm from the histogram of the particle size distribution (Figure 1f). It is expected that the large and smooth surface of these coin-like particles could be a good platform for growing $CoFe_2O_4$ nanospheres. Furthermore, if V is further increased to 1:1, the thickness of these coin-like particles decreases to 1.5−2.5 μm (named thinner coin-like, C3) while the diameter is unchanged (Figure 1e). It is noteworthy that the particle size distribution becomes wider and some irregular particles appear. The morphology transition between the flake- and coin-like particles can be well explained according to the Hansen solubility parameter (HSP) theory.[34,35] On the basis of previous similar research results, the solutions with different alcohol:water ratios will result in different Ra values, and these Ra values will decrease at first to a local minimum and finally increase again with a continuous increase in alcohol content. Meanwhile, the results also reveal that a smaller Ra value will responsible for the regular morphology. In that way, it can easily explain the fact that the initial high Ra value leads to the formation of the irregular flake-like particle and the decreased Ra value makes the particle shape more uniform and coin-like particles are formed, further increasing the Ra value that will change the particle shape back to inhomogeneous.

DOI: 10.1021/am508438s
ACS Appl. Mater. Interfaces 2015, 7, 4744−4750

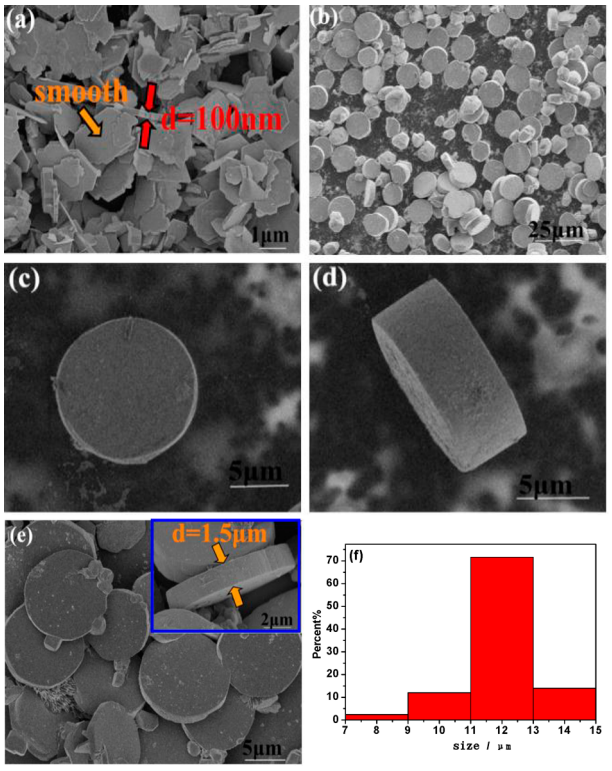

Figure 1. (a) SEM image of flake-like α-Fe_2O_3. (b–d) SEM images of coin-like α-Fe_2O_3. (e) SEM image of thinner coin-like α-Fe_2O_3. (f) Size distribution of coin-like α-Fe_2O_3.

Figure 2 reveals the XRD patterns of the starting material α-Fe_2O_3. Obviously, all the diffraction peaks at 23.78°, 33.05°,

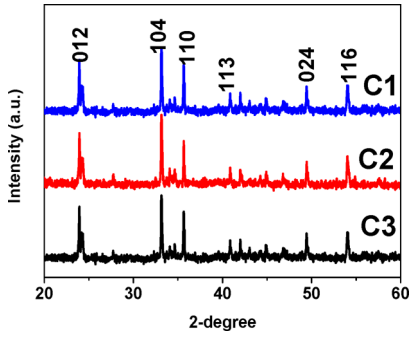

Figure 2. XRD diffraction patterns of flake-, coin-, and thinner coin-like α-Fe_2O_3.

35.61°, 40.75°, 49.45°, and 54.02° can be easily indexed to the (012), (104), (110), (113), (024), and (110) peaks of α-Fe_2O_3 (JCPDS Card No. 33-0664), respectively. However, the high temperature and the pressure during the solvothermal process may generate the Ba ferrite, as shown in the presence of a diffraction peak [beside the (012) peak of Fe_2O_3]. To prove the probable presence of Ba, the coin-like Fe_2O_3 has been tested by ICP. The result shows that the concentrations of Ba and Fe are 11.2 and 74.5 mg/L, respectively, corresponding to an atomic ratio of 0.061. However, the diffraction peak of Ba ferrite is so weak that it can be neglected.

To explore the role of $Ba(NO_3)_2$ in the reaction procedure, we conducted an additional experiment ($V_{PEG\text{-}200/distilled}$ = 1:3) without adding $Ba(NO_3)_2$. From Figure 3a, we easily find that

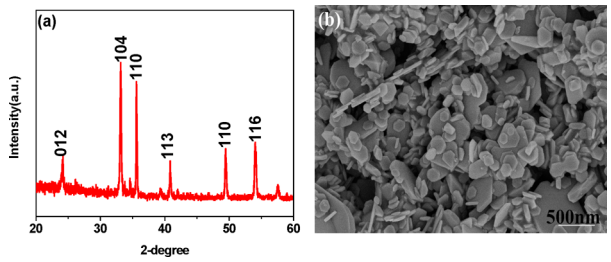

Figure 3. (a) XRD patterns and (b) FE-SEM of the sample prepared without adding $Ba(NO_3)_2$.

the diffraction peaks still belonged to α-Fe_2O_3 (JCPDS Card No. 33-0664). Meanwhile, the impurity peak beside (012) disappeared, which indirectly proved that such an impurity may result from Ba ferrite. Subsequently, the SEM image shows that the as-prepared Fe_2O_3 presents a flake-like structure with a size that ranged from 100 to 500 nm, which is much smaller than that of coin-like Fe_2O_3. At the same time, most of the flake-like Fe_2O_3 exhibits a tendency toward hexagonal structure. Thus, we may deduce that during the solvothermal process, $Ba(NO_3)_2$ may contribute to the enlargement of flake Fe_2O_3. At the same time, with the assistance of $Ba(NO_3)_2$, the hexagonal-like structure is turned to a coin-like structure.

To prepare the Fe_2O_3@$CoFe_2O_4$ composite, 0.2 g of the as-prepared α-Fe_2O_3 was added to the EG solvent for the solvothermal process, with $Co(Ac)_2$ and $FeCl_3$ as the precursors. Interestingly, the coin-like structure is completely covered by $CoFe_2O_4$ as shown in Figure 4a. Via the close-up views in panels b and c of Figure 4, we find that the coating layer consists of numerous nanospheres with an average diameter of ~70 nm. Figure 4d displays the TEM image of

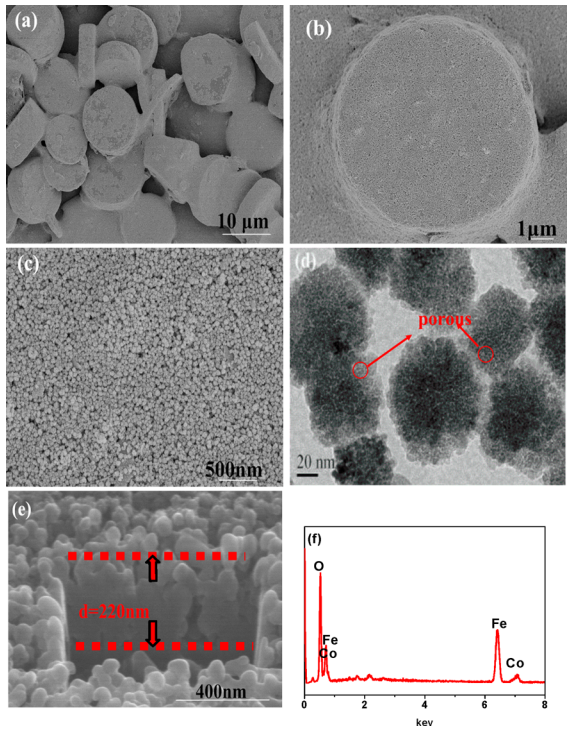

Figure 4. (a–c) SEM images of the coin-like Fe_2O_3@$CoFe_2O_4$ composite. (d) TEM image of $CoFe_2O_4$. (e) FIB image of the Fe_2O_3@$CoFe_2O_4$ composite. (f) EDX pattern of the coin-like composite.

DOI: 10.1021/am508438s
ACS Appl. Mater. Interfaces 2015, 7, 4744–4750

the composites; it is consistent with Figure 4b that the $CoFe_2O_4$ has a sphere-like structure. However, the white region marked in each $CoFe_2O_4$ nanosphere demonstrates that $CoFe_2O_4$ exhibits a porous structure. The thickness of the shell is ~220 nm as displayed in Figure 4e. The EDX spectrum is proof of the presence of Co and Fe together with elemental O in the composite (Figure 4f).

The XRD pattern of the representative coin-like Fe_2O_3@$CoFe_2O_4$ composite is shown in Figure 5. After the sample had

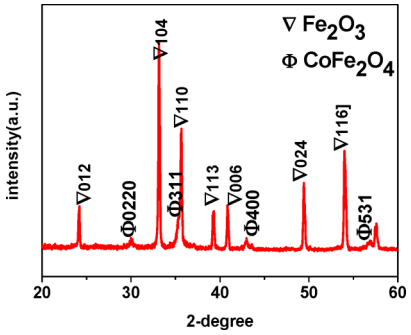

Figure 5. XRD patterns of the coin-like composite.

been coated with a $CoFe_2O_4$ layer, new diffraction peaks appeared at 29.91°, 35.31°, 43.01°, and 65.61°; they can be indexed into the cubic phase of $CoFe_2O_4$ (JCPDS Card No. 22-1086), while the intrinsic peaks of α-Fe_2O_3 are almost unchanged, indicating that $CoFe_2O_4$ successfully coats the surface of the coin-like form without altering the phase structure of α-Fe_2O_3.

The X-ray photoelectron spectrum was also recorded to compare the oxidation states of the coin-like α-Fe_2O_3 and its composite. From Figure 6a, the binding energy values of Fe

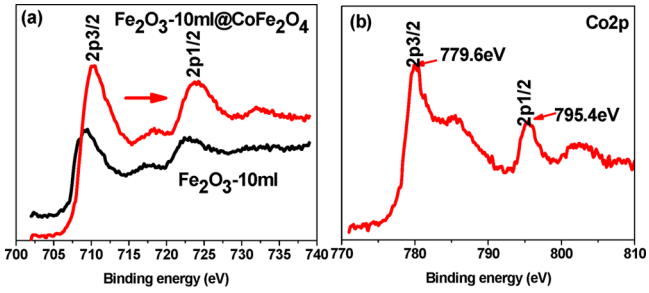

Figure 6. XPS spectra of (a) Fe 2p for coin-like α-Fe_2O_3 and its composite and (b) Co 2p for the coin-like composite.

$2p_{3/2}$ and $2p_{1/2}$ are located at 709.1 and 723.1 eV, respectively, which agree with the XPS results published by Sun et al. for α-Fe_2O_3.[36] For Fe 2p in the Fe_2O_3@$CoFe_2O_4$ composite, the values were 710.4 and 724.1 eV, respectively, slightly higher than those of pure α-Fe_2O_3. Furthermore, the opposite tendency is exhibited by Co 2p, for which binding energy values are observed at 779.6 and 795.4 eV, respectively, in the composite, slightly lower than those of pure $CoFe_2O_4$ [780.3 and 795.8 eV, respectively (see Figure 6b)].[37] Such a chemical shift for Fe 2p and Co 2p may originate from the interaction between Fe_2O_3 and $CoFe_2O_4$.[38,39] Specifically, the electronegativity value of elemental Fe is 1.83, slightly smaller than that of elemental Co (1.88). After $CoFe_2O_4$ had been coated on the surface of Fe_2O_3, the electron density of Fe is weakly affected by the attraction of Co, which resulted in the increase in the level of electron polarization of Fe−Co. Thus, the corresponding values of Fe 2p shift to a higher-energy region while those of Co 2p to a lower-energy region.[40]

The magnetic hysteresis loops of Fe_2O_3@$CoFe_2O_4$ composites were tested by a vibrating sample magnetometer as shown in Figure 7. It is clearly seen that the composites show novel

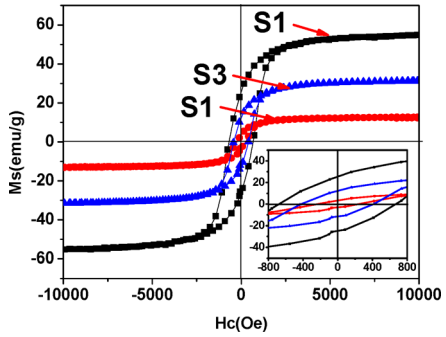

Figure 7. Hysteresis loops of the flake-, coin-, and thinner coin-like composites.

ferromagnetism due to the entry of $CoFe_2O_4$ into the composite. The magnetization of flake-like composite S1 (54 emu/g) is much higher than the values for the coin-like (19 emu/g) and thinner coin-like (33 emu/g) forms. The difference in magnetization values is related to the specific surface area of α-Fe_2O_3. Compared with the large size of coin-like Fe_2O_3, the flake-like Fe_2O_3 composite has a larger specific area. Under identical conditions, this composite can introduce more and more $CoFe_2O_4$ nanospheres. As far as the coercivity force (Hc) is concerned, it is well know that Hc is a vital parameter for assessing the magnetic properties, and the absorbent with a high Hc value may cause a high-frequency resonance.[41] Moreover, the Hc value is strongly related to grain size, and a small grain size may lead to a high coercivity.[42] Herein, the flake-like composite with the smallest size has the largest coercive force of 673 Oe, compared with those of the coin-like (S2) and thinner coin-like (S3) α-Fe_2O_3.

Figure 8 shows the calculated reflection loss values of the α-Fe_2O_3. The pure α-Fe_2O_3 with different morphologies exhibits poor microwave properties at coating thicknesses of 1.5−3 mm. It can be found from Figure 8a that the minimal reflection values of C1 (flake-like α-Fe_2O_3) increase with increasing thickness. The RL_{min} value of −6.3 dB is obtained at 14 GHz with a thickness of 3.0 mm. Such poor absorption properties also occur for other two kinds of α-Fe_2O_3 as seen in panels b and c of Figure 8, with an RL_{min} value of −7.2 dB for the coin-like form (C2) and −2.5 dB for the thinner coin-like form (C3) with the same thickness of 3 mm. In fact, the pure $CoFe_2O_4$ still performed badly in microwave absorption according to the recent literature; the pure RL_{min} value of the $CoFe_2O_4$ was less than −5 dB with a coating thickness of 2−5 mm.[37]

After samples had been coated with $CoFe_2O_4$ nanospheres, the microwave absorption properties of three kinds of composites are significantly improved in terms of the minimal value and frequency width, as described in Figure 9. Meanwhile, all of the composites present the same tendency in that the optimal RL peaks are shifted to the lower-frequency region with an increase in thickness, according to the equation[43]

$$t_m = nc/4f_m(\varepsilon_r\mu_r)^{1/2}$$

DOI: 10.1021/am508438s
ACS Appl. Mater. Interfaces 2015, 7, 4744−4750

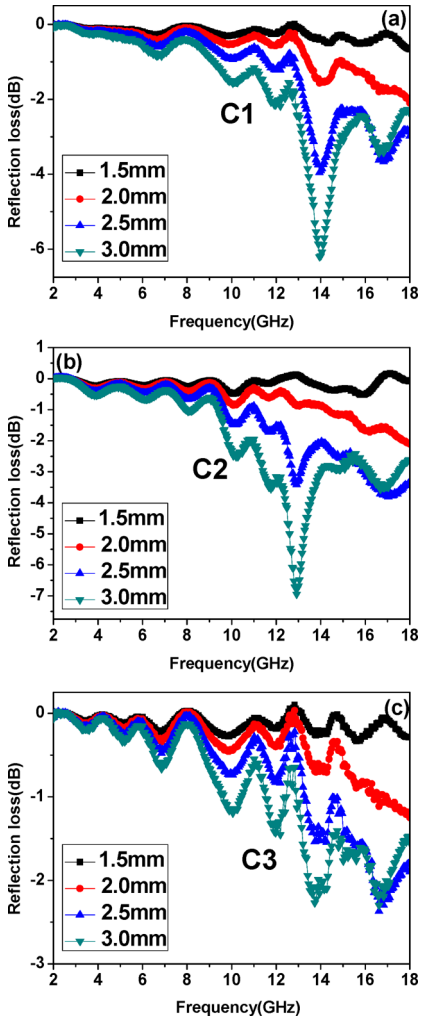

Figure 8. Reflection loss curves for the (a) the flake-like α-Fe_2O_3, (b) the coin-like α-Fe_2O_3, and (c) the thinner coin-like α-Fe_2O_3.

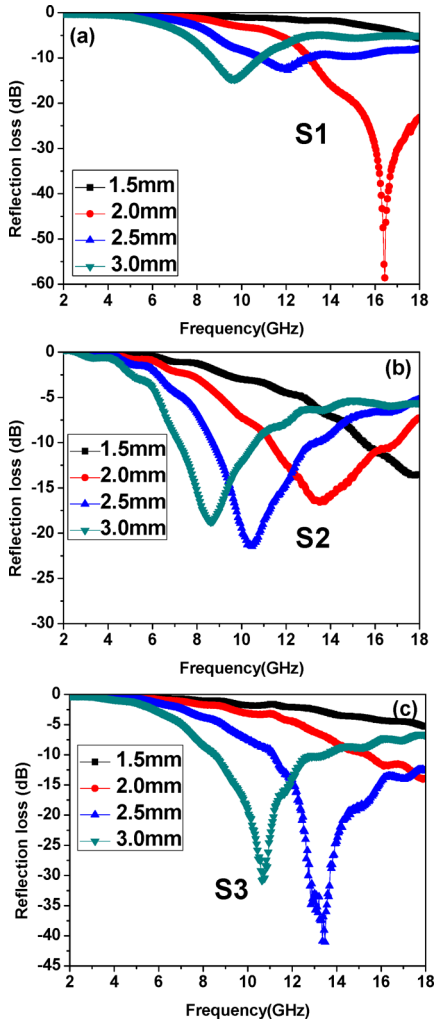

Figure 9. Reflection loss curves of (a) the flake-like α-Fe_2O_3 composite, (b) the coin-like α-Fe_2O_3 composite, and (c) the thinner coin-like α-Fe_2O_3 composite.

where t_m and f_m represent the matching thickness and frequency of a RL peak, respectively, μ_r and ε_r are the complex permeability and permittivity at a matching frequency, respectively, and C is the velocity of light. It is worth mentioning that S1 with a thickness of 2 mm presents an optimal RL_{min} of −60 dB at 16.3 GHz, which is much higher than the values of other types of Fe_2O_3- or $CoFe_2O_4$-based composites. Furthermore, the frequency bandwidth of less than −10 dB (comparable to 90% attenuation of incidence EM; thus, the value of less than −10 dB is considered to be an ideal value) reaches 5 GHz (13−18 GHz), which will easily meet the requirements of being lightweight and having an absorption intensity and a broad frequency. The RL data of coin- and thinner coin-like composite are displayed in panels b and c of Figure 9. Also, the enhanced absorption properties can be found in these two types of composites; S2 shows the optimal value of −23 dB with a thickness of 2.5 mm, while the minimal reflection loss value of S3 is up to −41 dB with a thickness of 2.5 mm. Furthermore, with a coating thickness of just 2 mm (in practical application, the coating thickness should be <2 mm), both coin- and thinner coin-like forms exhibit better absorption. For example, the coin-like form has an RL_{min} value of −17 dB with a bandwidth of 5.5 GHz (11.3−16.8 GHz), but S3 has an RL_{min} value that reaches −14 dB with a frequency bandwidth of 2.6 GHz (15.4−18 GHz).

We investigated the electromagnetic parameters of α-Fe_2O_3 and its composites to reveal the enhanced microwave absorption mechanism. It is clearly seen in Figure 10a that all forms of α-Fe_2O_3 have lower ε' values (approximately 4.3−3.8). Such a low value may lead to high impedance matching behavior. However, the α-Fe_2O_3 with a lower ε'' value has almost no ability to attenuate the incidence electromagnetic wave. When the $CoFe_2O_4$ was coated on the surface of the α-Fe_2O_3 (Figure 10b), apparent improved ε' values among the composites were found compared with those of the α-Fe_2O_3. At the same time, the novel increase in ε'' values not only maintains the good impedance matching behavior but also makes contributions to EM attenuation.

These special core−shell structures also make an important contribution to the microwave absorption properties. In Figure 11, we find that the high impedance matching of α-Fe_2O_3 can arouse more and more incidences of the electromagnetic wave passing into the absorber, but it is difficult to attenuate the electromagnetic wave by the lower ε'' value of α-Fe_2O_3; thus, most of the electromagnetic wave is reflected via transmission from the internal α-Fe_2O_3. As for the composites, this composite has a good impedance matching condition (despite the fact that a slightly increased ε' value may decrease the impedance properties, while the increase in the μ' and ε'' values

DOI: 10.1021/am508438s
ACS Appl. Mater. Interfaces 2015, 7, 4744−4750

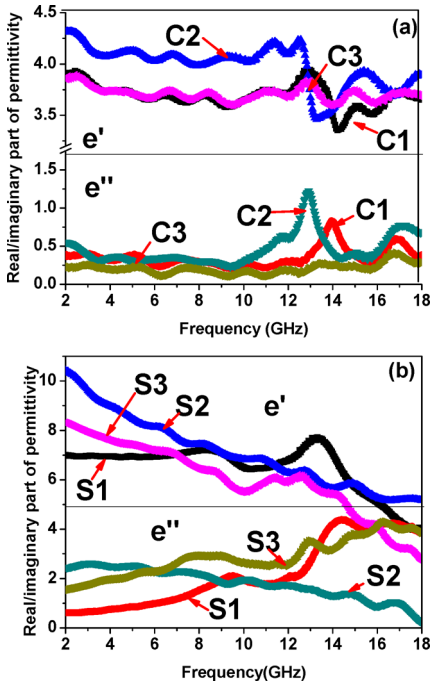

Figure 10. Electromagnetic characteristics (real/imaginary part of permittivity) of (a) three types of α-Fe_2O_3 and (b) three types of composites.

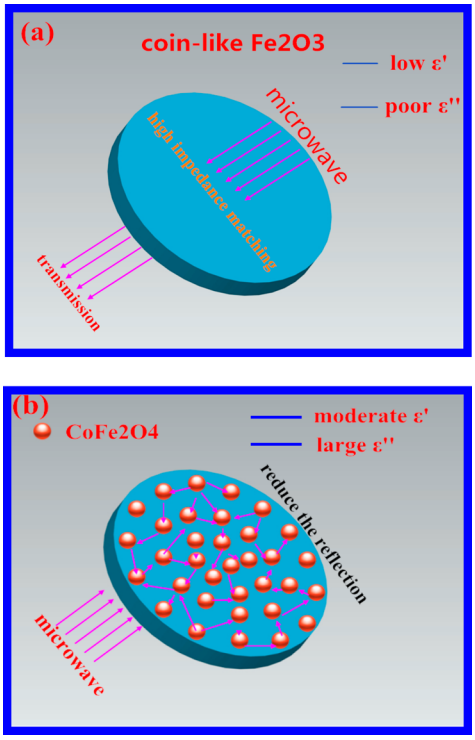

Figure 11. Schematic illustration of the absorption mechanism of (a) α-Fe_2O_3 and (b) Fe_2O_3@$CoFe_2O_4$ composites.

also can increase the impedance matching), which can let most of the incident EM wave go into the materials and be absorbed by the material itself. Meanwhile, because of the coating layer of the spherical $CoFe_2O_4$ ferrite particles, the rest of the incident EM wave will undergo a multireflection at the surface and can be further absorbed, as well.

4. CONCLUSION

In summary, three kinds of Fe_2O_3@$CoFe_2O_4$ composites, including flake-, coin-, and thinner coin-like structures, have been prepared by an efficient two-step solvothermal process. The Ra value of the mixed solvent (PEG-200/distilled water) has played a crucial role in the original α-Fe_2O_3 morphology. We compared the microwave absorption properties of α-Fe_2O_3 and Fe_2O_3@$CoFe_2O_4$ composites and found that all of the α-Fe_2O_3-based composites exhibit remarkable enhancements in both the RL value and frequency bandwidth. In particular, the flake-like composite has an optimal RL value of −60 dB, the bandwidth is up to 5 GHz, and the thickness was just 2 mm. The enhanced microwave absorption properties of the composites have been discussed in this paper. On one hand, the synergy effect between the core and shell may increase the extent of electron polarization. On the other, the high impedance matching of the composites can lead to strong absorption. Then, the incidence of the electromagnetic wave is apt to scatter among the porous $CoFe_2O_4$ nanospheres. These kinds of composites have potential applications in intensity absorption, lightweight, and broad frequency absorbents.

AUTHOR INFORMATION

Corresponding Authors

*E-mail: bszhang@nju.edu.cn.
*E-mail: gbji@nuaa.edu.cn.

Notes

The authors declare no competing financial interest.

ACKNOWLEDGMENTS

The financial support of the Aeronautics Science Foundation of China (2014ZF52072), the National Natural Science Foundation of China (51172109 and 11475086), and the Fundamental Research Funds for the Central Universities (3082014NS2014057) is gratefully acknowledged.

REFERENCES

(1) Song, W. L.; Cao, M. S.; Fan, L. Z.; Lu, M. M.; Li, Y.; Wang, C. Y.; Ju, H. F. Highly Ordered Porous Carbon/Wax Composites for Effective Electromagnetic Attenuation and Shielding. *Carbon* **2014**, *77*, 130−142.
(2) Wang, X.; Xu, X. J.; Gong, W.; Feng, Z. K.; Gong, R. Z. Electromagnetic Properties Fe-Si-Al/$BaTiO_3$/$Nd_2Fe_{14}B$ Particulate Composites at Microwave Frequencies. *J. Appl. Phys.* **2014**, *115*, 17C722−17C724.
(3) Wang, T.; He, J. P.; Zhou, J. H.; Tang, J.; Guo, Y. X.; Ding, X. C.; Wu, S. C.; Zhao, J. Q. Microwave Absorption Properties and Infrared Emissivities of Ordered Mesoporous C-TiO_2 Nanocomposites with Crystalline Frame Work. *J. Solid State Chem.* **2010**, *183*, 2797−2804.
(4) Zong, M.; Huang, Y.; Zhao, Y.; Sun, X.; Qu, C. H.; Luo, D. D.; Zheng, J. B. Facile Preparation, High Microwave Absorption and Microwave Absorbing Mechanism of RGO-Fe_3O_4 Composites. *RSC Adv.* **2013**, *3*, 23638−23648.
(5) Li, N.; Hu, C. W.; Cao, M. H. Enhanced Microwave Absorbing Performance of CoNi Alloy Nanoparticles Anchored on a Spherical Carbon Monolith. *Phys. Chem. Chem. Phys.* **2013**, *15*, 7685−7689.
(6) Lv, H. L.; Ji, G. B.; Wang, M.; Shang, C. M.; Zhang, H. Q.; Du, Y. W. FeCo/ZnO Composites with Enhancing Microwave Absorbing Properties: Effect of Hydrothermal Temperature and Time. *RSC Adv.* **2014**, *4*, 57529−57533.
(7) Wei, W.; Yue, X. G.; Zhou, Y.; Chen, Z.; Fang, J. Y.; Gao, C.; Jiang, Z. H. New Promising Hybrid Materials for Electromagnetic Interference Shielding with Improved Stability and Mechanical Properties. *Phys. Chem. Chem. Phys.* **2013**, *15*, 21043−21050.

DOI: 10.1021/am508438s
ACS Appl. Mater. Interfaces 2015, 7, 4744−4750

(8) Guo, J. L.; Wang, X. L.; Miao, P. L.; Liao, X. P.; Zhang, W. H.; Shi, B. One-Step Seeding Growth of Controllable Ag@Ni Core−Shell Nanoparticles on Skin Collagen Fiber with Introduction of Plant Tannin and Their Application in High-Performance Microwave Absorption. *J. Mater. Chem.* **2012**, *3*, 11933−11942.
(9) Duan, Y. P.; Liu, Z.; Jing, H.; Zhang, Y. H.; Li, S. Q. Novel Microwave Dielectric Response of Ni/Co-Doped Manganese Dioxides and Their Microwave Absorbing Properties. *J. Mater. Chem.* **2012**, *22*, 18291−18299.
(10) Yang, Z. H.; Li, Z. W.; Yu, L. H.; Yang, Y. H.; Xu, Z. H. Achieving High Performance Electromagnetic Wave Attenuation: A Rational Design of Silica Coated Mesoporous Iron Microcubes. *J. Mater. Chem. C* **2014**, *2*, 7583−7588.
(11) Yan, L. G.; Wang, J. B.; Han, X. H.; Ren, Y.; Liu, Q. F.; Li, F. S. Enhanced Microwave Absorption of Fe Nanoflakes after Coating with SiO_2 nanoshell. *Nanotechnology* **2010**, *2*, 095798−095802.
(12) Wang, Z. J.; Wu, L. N.; Zhou, J. G.; Shen, B. Z.; Jiang, Z. H. Enhanced Microwave Absorption of Fe_3O_4 Nanocrystals after Heterogeneously Growing with ZnO Nanoshell. *RSC Adv.* **2013**, *3*, 3309−3315.
(13) Liu, J. W.; Xu, J. J.; Che, R. C.; Chen, H. J.; Liu, M. M.; Liu, Z. W. Hierarchical Fe_3O_4@TiO_2 Yolk-Shell Microspheres with Enhanced Microwave-Absorption Properties. *Chem.—Eur. J.* **2013**, *19*, 6746−6752.
(14) Zhu, C. L.; Zhang, M. L.; Qiao, Y. J.; Xiao, G.; Zhang, F.; Chen, Y. J. Fe_3O_4/TiO_2 Core/Shell Nanotubes: Synthesis and Magnetic and Electromagnetic Wave Absorption Characteristics. *J. Phys. Chem. C* **2010**, *114*, 16229−16235.
(15) Liu, J. W.; Che, R. C.; Chen, H. J.; Zhang, F.; Xia, F.; Wu, Q. S.; Wang, M. Microwave Absorption Enhancement of Multifunctional Composite Microspheres with Spinel Fe_3O_4 Cores and Anatase TiO_2 Shells. *Small* **2012**, *8*, 1214−1221.
(16) Zhou, W. C.; Hu, X. J.; Bai, X. X.; Zhou, S. Y.; Sun, C. H.; Yan, J.; Chen, P. Synthesis and Electromagnetic, Microwave Absorbing Properties of Core-Shell Fe_3O_4-Poly(3,4-ethylenedioxythiophene) Microspheres. *ACS Appl. Mater. Interfaces* **2011**, *3*, 3839−3845.
(17) Han, Z.; Li, D.; Wang, H.; Liu, X. G.; Li, J.; Geng, D. Y.; Zhang, Z. D. Broadband Electromagnetic-wave Absorption by FeCo/C Nanocapsules. *Appl. Phys. Lett.* **2009**, *95*, 023114−023116.
(18) Li, Y.; Kim, Y. J.; Kim, A. Y.; Lee, K. J.; Jung, M. H.; Hur, N. H.; Park, K. H.; Seo, W. S. Highly Stable and Magnetically Recyclable Mesoporous Silica Spheres Embedded with FeCo/Graphitic Shell Nanocrystals for Supported Catalysts. *Chem. Mater.* **2011**, *23*, 5398−5403.
(19) Zhang, X. J.; Wang, G. S.; Cao, W. Q.; Wei, Y. Z.; Liang, J. F.; Guo, L.; Cao, M. S. Enhanced Microwave Absorption Property of Reduced Graphene Oxide (RGO)-$MnFe_2O_4$ Nanocomposites and Polyvinylidene Fluoride. *ACS Appl. Mater. Interfaces* **2014**, *6*, 7471−7478.
(20) Fu, M.; Jiao, Q. Z.; Zhao, Y. Preparation of $NiFe_2O_4$ Nanorod-Graphene Composites via an Ionic Liquid Assisted One-Step Hydrothermal Approach and Their Microwave Absorbing Properties. *J. Mater. Chem. A* **2013**, *1*, 5577−5586.
(21) Fu, M.; Jiao, Q. Z.; Zhao, Y.; Li, H. S. Vapor Diffusion Synthesis of $CoFe_2O_4$ Hollow Sphere/Graphene Composites as Absorbing Materials. *J. Mater. Chem. A* **2014**, *2*, 735−744.
(22) Ren, Y. L.; Zhu, C. L.; Zhang, S.; Li, C. Y.; Chen, Y. J.; Gao, P.; Yang, P. P.; Ouyang, Q. Y. Three-Dimensional SiO_2@Fe_3O_4 Core/Shell Nanorod Array/Graphene Architecture: Synthesis and Electromagnetic Absorption Properties. *Nanoscale* **2013**, *5*, 12296−12303.
(23) Ren, Y. L.; Zhu, C. L.; Qi, L. H.; Gao, H.; Chen, Y. J. Growth of γ-Fe_2O_3 Nanosheet Arrays on Graphene for Electromagnetic Absorption Applications. *RSC Adv.* **2014**, *4*, 21510−21516.
(24) Castel, V.; Brosseau, C.; Youssef, J. B. Magnetoelectric Effect in $BaTiO_3$/Ni Particulate Nanocomposites at Microwave Frequencies. *J. Appl. Phys.* **2009**, *106*, 064315−064329.
(25) Ghosh, S.; Bhattacharyya, S.; Kaiprath, Y.; Srivastava, K. V. Bandwidth-Enhanced Polarization-Insensitive Microwave Metamaterial Absorber and Its Equivalent Circuit Model. *J. Appl. Phys.* **2014**, *115*, 104503−104508.
(26) Zhang, H.; Xie, A. J.; Wang, C. P.; Wang, H. S.; Shen, Y. H.; Tian, X. Y. Novel γ-GO/α-Fe_2O_3 Composite Hydrogel: Synthesis, Characterization and High Performance of Electromagnetic Wave Absorption. *J. Mater. Chem. A* **2013**, *1*, 8547−8552.
(27) Chen, Y.; Liu, X. Y.; Mao, X. Y.; Zhuang, Q. X.; Xie, Z.; Han, Z. γ-Fe_2O_3-MWNT/Poly(P-Phenylenebenzobisoxazole) Composites with Excellent Microwave Absorption Performance and Thermal Stability. *Nanoscale* **2014**, *6*, 6440−6447.
(28) Ren, Y.; Zhu, C.; Qi, L.; Gao, H.; Chen, Y. J. Growth of γ-Fe_2O_3 Nanosheet Arrays on Graphene for Electromagnetic Absorption Applications. *RSC Adv.* **2014**, *4*, 21510−21516.
(29) Wu, H.; Wang, L. D.; Wu, H. J.; Lian, Q. Synthesis and Significantly Enhanced Microwave Absorption Properties of Hematite Dendrites/Polyaniline Nanocomposite. *Appl. Phys. A: Mater. Sci. Process.* **2014**, *115*, 1299−1307.
(30) Sandip, M.; Shrivastava, N. K.; Suin, S.; Khatua, B. B. Polystyrene/MWCNT/Graphite Nanoplate Nanocomposites: Efficient Electromagnetic Interference Shielding Material Through Graphite Nanoplate-MWCNT-Graphite Nanoplate Networking. *ACS Appl. Mater. Interfaces* **2013**, *5*, 4712−4724.
(31) Anil, O.; Kuldeep, S.; Amita, C.; Sundeep, K. D. Microwave Absorption Behavior of Core-Shell Structured Poly(3,4-Ethylenedioxythiophene)-Barium Ferrite Nanocomposites. *ACS Appl. Mater. Interfaces* **2010**, *2*, 927−933.
(32) Melvin, G. J. H.; Ni, Q. Q.; Narsuki, T. Electromagnetic Wave Absorption Properties of Barium Titanate/Carbon Nanotube Hydrid Nanocomposites. *J. Alloys Compd.* **2014**, *615*, 84−90.
(33) Ji, R. L.; Cao, C. B.; Chen, Z.; Zhai, H. Z.; Bai, J. Solvothermal Synthesis of $Co_xFe_{3-x}O_4$ Spheres and Their Microwave Absorption Properties. *J. Mater. Chem. C* **2014**, *2*, 5944−5953.
(34) Jiang, X. L.; Wang, Y. L.; Li, M. G. Selecting Water-Alcohol Mixed Solvent for Synthesis of Polydopamine Nano-Spheres Using Solubility Parameter. *Sci. Rep.* **2014**, *4*, 06070−060704.
(35) Zhou, K. G.; Mao, N. N.; Wang, H. X.; Peng, Y.; Zhang, H. L. A Mixed-Solvent Strategy for Efficient Exfoliation of Inorganic Graphene Analogues. *Angew. Chem., Int. Ed.* **2011**, *50*, 10839−10842.
(36) Sun, G. B.; Dong, B. X.; Cao, H. B.; Wei, Q. C.; Hu, W. Hierarchical Dendrite-Like Magnetic Materials of Fe_3O_4, γ-Fe_2O_3, and Fe with High Performance of Microwave Absorption. *Chem. Mater.* **2011**, *23*, 1587−1593.
(37) Zong, M.; Huang, Y.; Wu, H. W.; Zhao, Y.; Wang, Q. F.; Sun, X. One-Pot Hydrothermal Synthesis of RGO/$CoFe_2O_4$ Composite and Its Excellent Microwave Absorption Properties. *Mater. Lett.* **2014**, *114*, 52−55.
(38) Sun, J. X.; Yuan, Y. P.; Qiu, L. G.; Jiang, X.; Xie, A. J.; Shen, Y. H.; Zhu, J. F. Fabrication of Composite Photocatalyst γ-C_3N_4-ZnO and Enhancement of Photocatalytic Activity under Visible Light. *Dalton Trans.* **2012**, *41*, 6756−6763.
(39) Kumar, S.; Baruah, A.; Tonda, S.; Kumar, B.; Shanker, V.; Sreedhar, B. Cost-Effective and Eco-Friendly Synthesis of Novel and Stable N-Doped ZnO/g-C_3N_4 Core-Shell Nanoplates with Excellent Visible-Light Responsive Photocatalysis. *Nanoscale* **2014**, *6*, 4830−4842.
(40) Du, P.; Song, L. X.; Xia, J.; Teng, Y.; Yang, Z. K. Construction and Application of α-Fe_2O_3 Nanocubes Dominated by the Composite Interaction between Polyvinyl Chloride and Potassium Ferrocyanide. *J. Mater. Chem. A* **2014**, *2*, 11439−11447.
(41) Ohkoshi, S.; Kuroki, S.; Sakurai, S.; Matsumoto, K.; Sato, K.; Sasaki, S. A Millimeter-wave Absorber Based on Gallium-Substituted ε-Iron Oxide Nanomagnet. *Angew. Chem., Int. Ed.* **2007**, *46*, 8392−8395.
(42) Herzer, G. Modern soft magnets: Amorphous and Nanocrystalline Materials. *Acta Mater.* **2013**, *61*, 718−734.
(43) Zhang, H. M.; Zhu, C. L.; Chen, Y. J.; Gao, H. Growth of Fe_3O_4 Nanorod Arrays on Graphene Sheets for Application in Electromagnetic Absorption Fields. *ChemPhysChem* **2014**, *15*, 2261−2266.

DOI: 10.1021/am508438s
ACS Appl. Mater. Interfaces 2015, 7, 4744−4750